

A novel approach to correcting T_e -based mass-metallicity relations

Alex J. Cameron,^{*} Harley Katz, and Martin P. Rey

Sub-department of Astrophysics, University of Oxford, Keble Road, Oxford OX1 3RH, United Kingdom

Accepted XXX. Received YYY; in original form ZZZ

ABSTRACT

Deriving oxygen abundances from the electron temperature (hereafter the T_e -method) is the gold-standard for extragalactic metallicity studies. However, unresolved temperature fluctuations in H II regions can bias metallicity estimates low, with a magnitude that depends on the underlying and typically unknown temperature distribution. Using a toy model, we confirm that computing T_e -based metallicities using the temperature derived from the [O III] $\lambda 4363/\lambda 5007$ ratio (‘ratio temperature’; T_{ratio}) results in an underprediction of metallicity when temperature fluctuations are present. In contrast, using the unobservable ‘line temperatures’ (T_{line}) that provide the mean electron and ion density-weighted emissivity yield an accurate metallicity estimate. To correct this bias, we demonstrate an example calibration of a relation between T_{ratio} and T_{line} based on a high-resolution (4.5 pc) RAMSES-RTZ simulation of a dwarf galaxy that self-consistently models the formation of multiple H II regions and ion temperature distribution in a galactic context. Applying this correction to the low-mass end of the mass-metallicity relation shifts its normalization up by 0.18 dex on average and flattens its slope from 0.87 to 0.58, highlighting the need for future studies to account for, and correct, this bias.

Key words: ISM: abundances – galaxies: abundances – galaxies: HII regions – galaxies: ISM – galaxies: evolution

1 INTRODUCTION

The gas-phase oxygen abundance (‘metallicity’ hereafter) of a galaxy is a fundamental property that encodes a wealth of information on its star formation, enrichment, and assembly history. Galaxy metallicity exhibits a tight correlation with stellar mass, the mass-metallicity relation (MZR; e.g. [Lequeux et al. 1979](#), [Tremonti et al. 2004](#)), with scatter in this relation correlating with star formation rate (e.g. [Ellison et al. 2008](#)) and gas mass (e.g. [Bothwell et al. 2013](#)). Measurements of the slope and normalisation of this relation are interpreted as the collective effect of metal-enriched outflows and metal-poor inflows (e.g. [Tremonti et al. 2004](#)), and used to constrain astrophysical models that predict the chemical enrichment and assembly histories of galaxies (e.g. [Ma et al. 2016](#)).

However, the exact shape of the MZR remains debated, as its slope and normalisation is sensitive to the technique used to measure metallicity (e.g. [Kewley & Ellison 2008](#); [Yates et al. 2020](#)). Using recombination lines (RL) is often considered the most robust metallicity estimate, due to its weak dependence on gas temperature and density. But it relies on measuring multiple faint metal lines, which is possible in the local neighbourhood of the Milky Way (e.g. [Peimbert et al. 1993](#); [Esteban et al. 2002](#)) but prohibitive for extragalactic samples. In contrast, strong-line methods rely only on ratios of the brightest emission lines and can therefore be widely applied. However, they need to be calibrated to more direct measurements (e.g. [Curti et al. 2017](#)) or theoretical predictions (e.g. [McGaugh 1991](#); [Kewley et al. 2019](#)), each associated with difficult-to-quantify systematic uncertainties ([Kewley & Ellison 2008](#)).

As a result, the T_e method ([Peimbert 1967](#)) has been the *de facto*

gold standard for measurements of the MZR (e.g. [Andrews & Martini 2013](#), hereafter [AM13](#); [Curti et al. 2020](#)). It relies on detecting auroral emission lines (e.g. [O III] $\lambda 4363$) to estimate T_e , enabling us to derive metallicities solely from line emissivities based on collision strengths from quantum mechanical calculations (e.g. [Palay et al. 2012](#)). Detecting such faint auroral lines is observationally challenging, but possible at low-redshift for large samples of individual low-metallicity galaxies (e.g. [Izotov et al. 2019](#)) or stacks of higher-metallicity galaxies ([Curti et al. 2017](#)). Further, the advent of the James Webb Space Telescope now allows us to make such detections at high-redshift (e.g. at $z = 8.5$; [Katz et al. 2022a](#); [Curti et al. 2022](#)). The central role played by the T_e -method to constrain chemical evolution across cosmic time makes it paramount to pinpoint its potential biases and losses of accuracy.

In fact, T_e -method metallicities are typically lower than RL techniques by as much as ~ 0.3 dex in observations where both can be computed (e.g. [Liu et al. 2001](#); [García-Rojas & Esteban 2007](#)). A promising explanation for these offsets is the presence of inhomogeneous temperature distributions, either within H II regions or integrated across a galaxy. The exponential scaling of line emissivities with temperature then biases the T_e -method metallicity measurements low ([Peimbert 1967](#); [Stasińska 2005](#); [Bresolin 2008](#); Section 2). T_e -metallicities can be debiased by measuring multiple temperatures for the same system to estimate the underlying distribution ([Peimbert & Costero 1969](#)), but such observations are typically not feasible for distant galaxies.

Pinpointing the importance of temperature fluctuations is thus essential to calibrate the true magnitude of this long-standing bias and recover accurate extragalactic T_e -metallicities. In this paper, we introduce a new physically-motivated model to achieve this aim. Rather than estimating temperature fluctuations from measurements of lo-

^{*} E-mail: alex.cameron@physics.ox.ac.uk

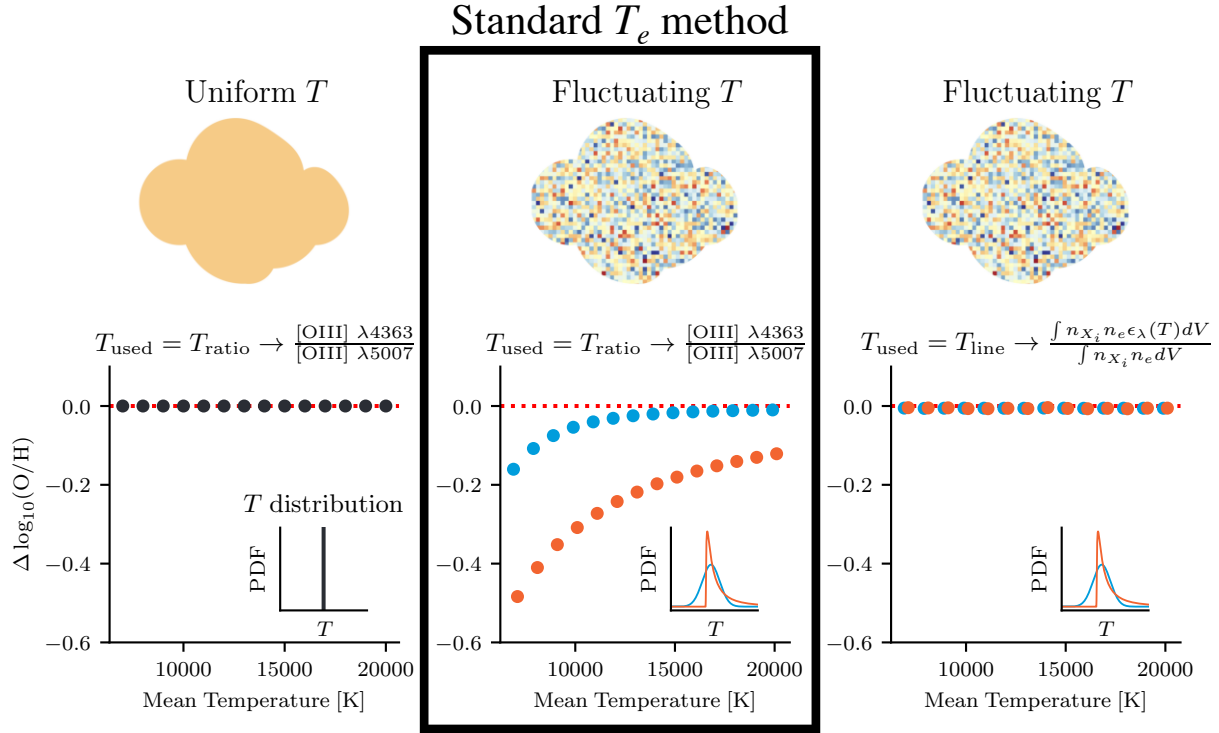


Figure 1. Toy-model demonstrating how temperature fluctuations bias the T_e -method when applied to a uniform metallicity system. From left to right, lower panels show the discrepancy between the true metallicity and that derived from Equation 1 for: a homogeneous cloud with uniform temperature and using T_{ratio} (the T_e inferred from $[\text{O III}] \lambda 4363/\lambda 5007$), a cloud with temperature fluctuations and using T_{ratio} , and a cloud with temperature fluctuations and using T_{line} (Equation 2). Temperature fluctuations are either normally (blue) or lognormally (orange) distributed (insets). The standard T_e -method (centre panel) always underpredicts metallicity when temperature fluctuations are present, with the deficit depending on the exact shape of the temperature distribution. In contrast, when the cloud is homogeneous or when T_{line} is used, the metallicity prediction is accurate.

cal H II regions (e.g. Kobulnicky et al. 1999) or photoionization models (Stasińska 1990; Garnett 1992), we use a high-resolution (≈ 4.5 pc) simulation of an isolated dwarf galaxy with multifrequency radiation-hydrodynamics coupled to non-equilibrium metal and molecular chemistry. This allows us to self-consistently predict the distribution of H II region temperatures, across an entire galaxy undergoing star formation and feedback episodes. We estimate the resulting bias in T_e metallicities (Section 3) and how it affects the derived MZR (Section 4).

2 HOW TEMPERATURE FLUCTUATIONS AFFECT TEMPERATURE BASED METALLICITIES

To gain insights into the importance of temperature fluctuations, we construct a toy model that derives T_e -metallicities from O II and O III emission lines which are readily available for extragalactic studies. Ionized oxygen and hydrogen trace each other in the ISM due to their near-identical ionization potentials and a strong coupling from charge exchange reactions. Assuming in these ionized regions that the O^+ and O^{++} ionization states dominate, the metallicity is:

$$\frac{\text{O}}{\text{H}} \approx \frac{\text{O}^+}{\text{H}^+} + \frac{\text{O}^{++}}{\text{H}^+} = \frac{L_{\lambda\lambda 3727}}{L_{\text{H}\beta}} \frac{\epsilon_{\text{H}\beta}(T_1)}{\epsilon_{\lambda\lambda 3727}(T_2)} + \frac{L_{\lambda 5007}}{L_{\text{H}\beta}} \frac{\epsilon_{\text{H}\beta}(T_3)}{\epsilon_{\lambda 5007}(T_4)}, \quad (1)$$

where $L_{\lambda 5007}$, $L_{\lambda\lambda 3727}$, and $L_{\text{H}\beta}$ are the observed luminosities of the $[\text{O III}] \lambda 5007$, $[\text{O II}] \lambda\lambda 3727$, and $\text{H}\beta$ lines, and $\epsilon_{\lambda 5007}$, $\epsilon_{\lambda\lambda 3727}$, and $\epsilon_{\text{H}\beta}$ are their emissivities.

The key to this calculation is the measurement of the temperature. It is typical to assume $T_3 = T_4$ and adopt the ratio temperature (T_{ratio}) measured from the $[\text{O III}] \lambda 4363/[\text{O III}] \lambda 5007$ ratio. Then $T_1 = T_2$ are

either measured from $[\text{O II}]$ auroral lines, or derived by assuming a relation between the O II and O III temperatures (e.g. Pérez-Montero 2017). Indeed, applying Equation 1 with T_{ratio} to a single parcel of gas with uniform temperature provides an unbiased estimate of the metallicity, which depends only on atomic physics (Figure 1, left).

However, when multiple parcels of gas with a range of temperatures are present, we can introduce the ‘line temperature’, T_{line} (e.g. Stasińska 1978):

$$\epsilon_{\lambda}(T_{\text{line}}) = \frac{\int n_{X_i} n_e \epsilon_{\lambda}(T) dV}{\int n_{X_i} n_e dV}, \quad (2)$$

where n_e is the electron density, n_{X_i} is the number density of species X_i with a transition that gives rise to an emission line with wavelength λ , and ϵ_{λ} is the emissivity of that line. T_{line} encodes the average emissivity of each emission line across the range of probed temperatures, weighted by the local electron and ion densities. The crux of the bias described in Section 1 is that, since the emissivity of $\text{H}\beta$, $[\text{O II}] \lambda\lambda 3727$, and $[\text{O III}] \lambda 5007$ scale differently with temperature, each line has a different T_{line} that can each differ from T_{ratio} . Hence using T_{ratio} in Equation 1 can result in an incorrect metallicity.

To gauge the magnitude of this effect, we setup a system comprised of 1,000 gas parcels, all with constant metallicity of $12 + \log_{10}(\text{O}/\text{H}) = 8.48$, randomized electron densities between $10^{-1} - 10^3 \text{ cm}^{-3}$, and randomized temperatures. We construct 28 systems assuming either a normal ($\sigma = 10^3 \text{ K}$) or lognormal ($\sigma = 0.3 \text{ dex}$) temperature distribution, each with 14 different mean temperature values ranging from 7,000 K to 20,000 K. Within each parcel, the gas temperature is the same for each ion. We then obtain

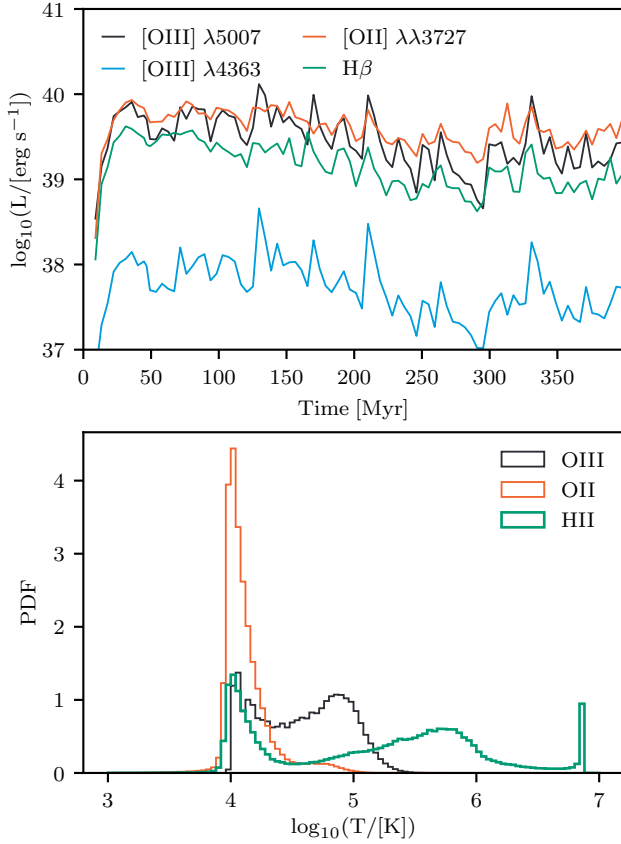


Figure 2. (Top) Evolution of the emission line luminosities needed to apply the [O III] T_e method as a function of time in the simulation. (Bottom) Example ion mass-weighted temperature distribution derived from the simulation at 400 Myr, showcasing the extended and non-trivial temperature distribution at a particular time.

the total luminosities of [O III] $\lambda 5007$, [O III] $\lambda 4363$, [O II] $\lambda \lambda 3727$, and H β by summing the emergent luminosities from each gas parcel. Applying the T_e -method, we compute the ‘measured’ metallicity of the system by deriving T_{ratio} from [O III] $\lambda 4363/\lambda 5007$ and inputting this into Equation 1. The centre panel of Figure 1 shows that metallicities derived using T_{ratio} systematically underpredict the true value, and the magnitude of the bias strongly depends on both the shape of the temperature distribution (blue versus orange) and its mean temperature (left to right). Since mean temperature is often correlated with metallicity, temperature fluctuations can affect *relative* metallicity measurements, and impact the shape of the MZR.

In contrast, if we adopt the corresponding T_{line} for each T_i in Equation 1, we obtain an unbiased metallicity measurement, regardless of the underlying temperature distribution (Figure 1 right panel). However, T_{line} is not a directly measurable quantity. Thus, we now present a new, physically-motivated method to convert T_{ratio} to T_{line} and debias T_e -derived metallicities.

3 QUANTIFYING TEMPERATURE FLUCTUATIONS IN A SIMULATED DWARF GALAXY

We now make use of novel numerical methods that allow us to directly predict the temperature distribution of H II regions within a simulated galaxy, and estimate a relation between T_{ratio} and T_{line} .

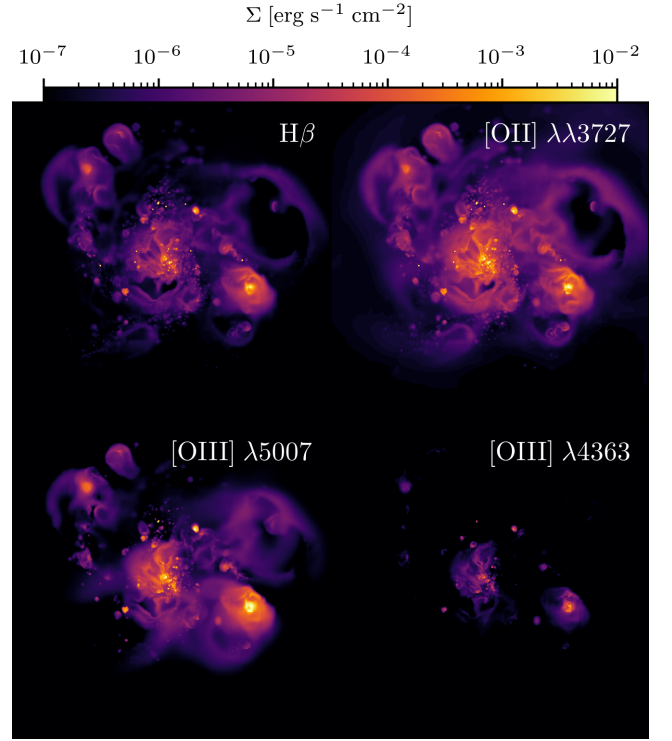


Figure 3. 4.5 kpc maps of H β , [O II] $\lambda \lambda 3727$, [O III] $\lambda 5007$, and [O III] $\lambda 4363$, surface brightness at $t = 400$ Myr, showing the spatial variations across H II regions at a given time.

3.1 Simulation methods

We simulate the same dwarf galaxy as in Katz (2022) with a halo mass of $10^{10} M_{\odot}$, a circular velocity of 30 km s^{-1} , a disk gas mass of $3.5 \times 10^8 M_{\odot}$, and an initial central metallicity of $10^{-1} Z_{\odot}$ (see Katz 2022, Section 4 for further details). We then evolve these initial conditions using the RAMSES-RTZ code (Katz 2022) and the PRISM interstellar (ISM) model for cooling and heating (Katz et al. *in prep.*).

Radiation hydrodynamics is self-consistently computed in eight energy bins (Kimm et al. 2017, Table 2), assuming a reduced speed of light ($c_{\text{sim}} = c/100$), and is coupled to the non-equilibrium chemistry of eight ionization states of O, seven of N, six of C, and six of Si, Mg, Fe, S, and Ne, and all ionization states of H and He. We account for star formation, stellar feedback and enrichment from massive stars (Katz 2022, Section 4), and apply a Haardt & Madau (2012) UV background which is exponentially suppressed at $\rho > 10^{-2} \text{ cm}^{-3}$. We employ a fixed cosmic-ray background ionization rate of $\eta_{\text{cr}} = 10^{-16} \text{ s}^{-1} \text{H}^{-1}$.

Our simulations achieve a resolution of 4.5 pc across the ISM, resolving the structure of large H II regions. Using the out-of-equilibrium temperatures, ionization states, and electron densities self-consistently produced by the simulation, we solve for equilibrium level populations to predict emission line luminosities. We follow Katz et al. (2022b) to compute Balmer lines according to the most recent atomic data in CHIANTI (Dere et al. 2019), while oxygen line luminosities are calculated with PyNEB (Luridiana et al. 2015).

3.2 Abundance discrepancy in our simulated galaxy

To provide the cleanest test of the T_e -method, we work only with the intrinsic luminosities so as to not introduce uncertainties due

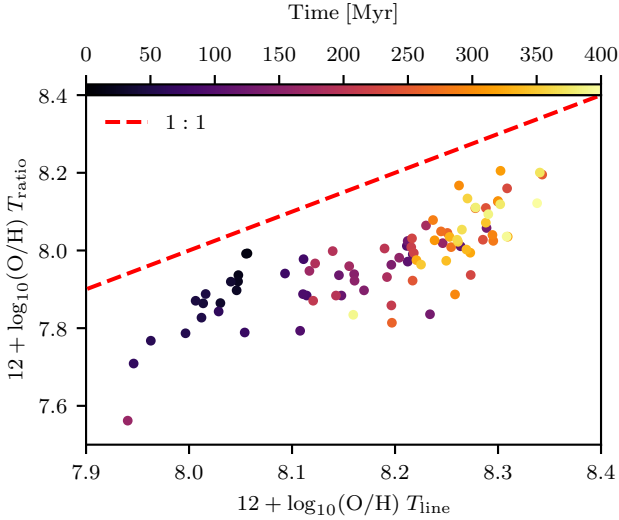


Figure 4. Metallicity measured with T_{line} vs. metallicity measured with T_{ratio} as a function of time. As the simulation progresses (colours), the metallicity of the galaxy grows but the T_{ratio} -derived metallicity always results in a systematically lower value.

to dust attenuation. This implicitly assumes that observations can be perfectly dust-corrected. Furthermore, we restrict ourselves to [O III] $\lambda 5007$, [O III] $\lambda 4363$, [O II] $\lambda \lambda 3727$, and $H\beta$ to provide a representative extragalactic experiment. [O II] $\lambda \lambda 7320, 7330$ auroral lines are extremely challenging to observe at high-redshift (e.g. Sanders et al. 2022), thus we assume for our analysis that the O II temperature cannot be directly calculated. We instead derive the O II temperature from the O III temperature using the relation from Pérez-Montero (2017) (their Equation 14) after verifying that this provides a good fit to our simulated data.

We evolve the galaxy for 400 Myr. After the initial starburst relaxes from the initial conditions, the star formation rate (SFR) fluctuates in the range $10^{-2} < \text{SFR}/M_{\odot}\text{yr}^{-1} < 10^{-1}$. These temporal fluctuations are reflected on the galaxy-integrated emission line luminosities needed for the T_e -method (Figure 2, top panel). We further show in the bottom panel of Figure 2 the ion mass-weighted temperature distributions for O III, O II, and H II at the end of the simulation, and emission-line maps (Figure 3). At a given time, the dynamic ISM environment generates an extended ion temperature distribution with non-trivial shape, and an irregular emission line spatial distribution. These temperature fluctuations will cause a bias in the T_e -method.

From the simulated [O III] $\lambda 5007$, [O III] $\lambda 4363$, [O II] $\lambda \lambda 3727$, and $H\beta$ luminosities, we then calculate metallicity using the standard direct method (Equation 1) using the ratio temperature derived from [O III] $\lambda 4363$ /[O III] $\lambda 5007$. We further compute the unobservable T_{line} (Equation 2) using the self-consistent simulated distribution of temperatures, electron and ion densities, and compare the derived metallicities between the two in Figure 4. Using T_{ratio} results in a systematic underprediction with an average deficit of 0.21 dex, ranging between 0.06 – 0.4 dex across the entire simulated time (colours). These offsets have comparable magnitude to discrepancies between T_e and RL metallicities (García-Rojas & Esteban 2007), and between global measurements compared to combining individual H II regions (Kobulnicky et al. 1999).

3.3 Calibrating the $T_{\text{line}}-T_{\text{ratio}}$ relation

Figure 5 shows the ratio temperature as measured from [O III] $\lambda 4363/\lambda 5007$ versus the line temperatures of [O III] $\lambda 5007$, [O II] $\lambda \lambda 3727$, and $H\beta$ for each time snapshot of our simulated galaxy between 50 and 400 Myr. The temperatures of all three lines are tightly correlated with T_{ratio} , such that

$$\begin{aligned} T_{\text{line, [OIII] } \lambda 5007} &= 0.60 T_{\text{ratio}} + 3258 \text{ K}, \\ T_{\text{line, [OII] } \lambda \lambda 3727} &= 0.065 T_{\text{ratio}} + 8859 \text{ K}, \text{ and} \\ T_{\text{line, H}\beta} &= 0.117 T_{\text{ratio}} + 8034 \text{ K}. \end{aligned} \quad (3)$$

We stress that these equations are obtained from a single simulated dwarf galaxy and should not be generalized blindly to the whole galaxy population. Nonetheless, they currently provide the most realistic estimate of temperature fluctuations across dwarf galaxies' H II regions, and we demonstrate in the next section how taking them into account could reshape the MZR.

4 DISCUSSION AND CONCLUSIONS

We have shown how temperature fluctuations within an H II region and throughout a galaxy can bias T_e -method metallicities low, with a magnitude that depends on the shape and mean of the underlying distribution. While the existence of this bias is well established (e.g. Peimbert 1967; Stasińska 2005), estimating its magnitude and correcting it in extragalactic samples is challenging (e.g. Peimbert 1967, AM13). We propose a new solution based on deriving a relation between the observable T_{ratio} (that can be derived from auroral-to-nebular line ratios) to the unobservable T_{line} , which we demonstrate provides a much more accurate temperature estimator for the T_e method (Figure 1).

We calibrate this relation using high-resolution (4.5 pc) numerical simulations of a dwarf galaxy with RAMSES-RTZ that couple non-equilibrium metal chemistry to multi-frequency radiation hydrodynamics to estimate the temperature distributions across H II regions. Applying the standard T_e -method to simulated data underpredicts the representative metallicity of H II regions at all times, by 0.21 dex on average and up to 0.4 dex (Figure 4). Nonetheless, each line temperature tightly correlates with T_{ratio} from [O III] (Figure 5), offering us the opportunity to debias metallicity estimates.

Our single simulation is unlikely to be fully representative of the wider galaxy population, and Equation 3 should be employed with caution. Nonetheless, we wish to assess how accounting for unresolved temperature fluctuations could impact the shape of the MZR. We thus use the stacked SDSS spectra from AM13 for stellar mass bins below $10^{8.5} M_{\odot}$, and apply the T_e -method from the [O III] $\lambda 4363$, [O III] $\lambda 5007$, [O II] $\lambda \lambda 3727$, and $H\beta$ fluxes. Figure 6 shows the resulting metallicities (black points), with the best fit (black line) using the functional form in AM13 (their Equation 5). The original fit to the MZR from AM13 (red line) shows minor differences due to their different atomic data, different relation to convert between T_e (O III) and T_e (O II), and their more extended stellar mass range for the fit.

We then use Equation 3 to estimate T_{line} for each emission line before deriving the metallicity from Equation 1 and recalculate the MZR (blue points). The metallicity increases at all stellar masses, with the stellar-mass dependent offset reaching ~ 0.3 dex for lower mass bins, and flattens the measured slope of the MZR from 0.87 to 0.58. Our experiment emphasizes that a careful quantification and correction of biases in metallicity measurements is essential to robustly interpret the MZR. We advocate for larger suites of comparable

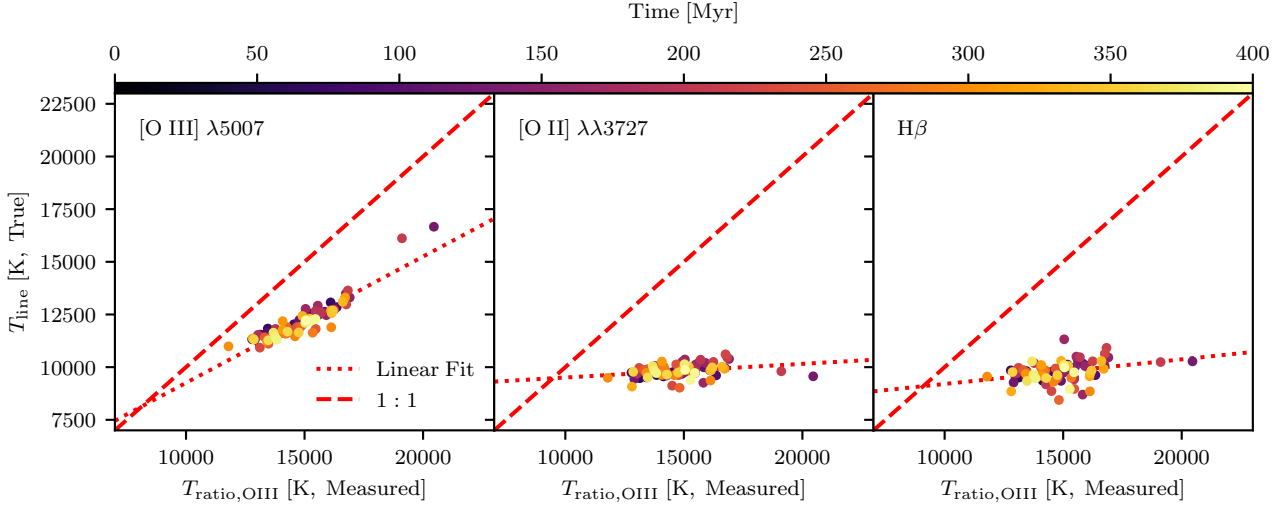


Figure 5. T_{ratio} from [O III] $\lambda 4363$ /[O III] $\lambda 5007$ compared to the [O III] $\lambda 5007$ (left), [O II] $\lambda \lambda 3727$ (centre), and H β (right) line temperatures. All T_{line} are systematically underpredicted by T_{ratio} , but they exhibit a tight correlation for each emission line.

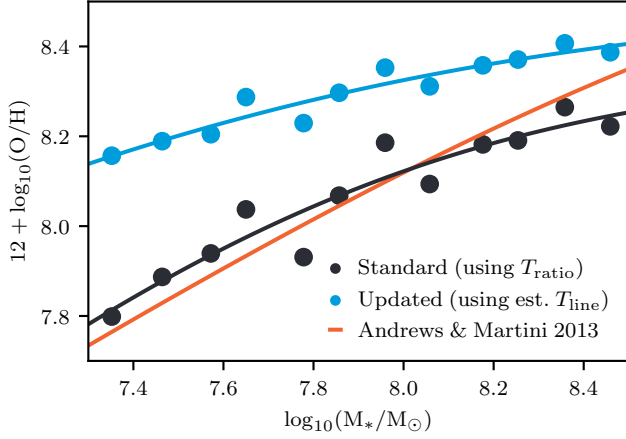


Figure 6. MZR for SDSS galaxies based on the standard T_e method using T_{ratio} (black), our updated T_e method using the estimated T_{line} (blue), and the fit from AM13 (red). The slope of the MZR flattens and the normalization increases using our new approach to debiasing the measurement.

simulations than used in this study, across a larger range of stellar masses and metallicities, and in a cosmological context. Constructing relations from such a suite of simulations could aid interpretations of observations in a manner comparable to how 1D photoionisation models (from e.g. CLOUDY or MAPPINGS) have historically been used.

ACKNOWLEDGEMENTS

This work was performed using the DiRAC Data Intensive service at Leicester, operated by the University of Leicester IT Services, which forms part of the STFC DiRAC HPC Facility. The equipment was funded by BEIS capital funding via STFC capital grants ST/K000373/1 and ST/R002363/1 and STFC DiRAC Operations grant ST/R001014/1. DiRAC is part of the National e-Infrastructure. AJC acknowledges funding from the ‘FirstGalaxies’ Advanced Grant from the European Research Council (ERC) under the European Union’s Horizon 2020 research and innovation programme (Grant

agreement No. 789056). MR is supported by the Beecroft Fellowship funded by Adrian Beecroft.

DATA AVAILABILITY

Underlying data will be shared on reasonable request to the authors.

REFERENCES

- Andrews B. H., Martini P., 2013, *ApJ*, **765**, 140
 Bothwell M. S., Maiolino R., Kennicutt R., Cresci G., Mannucci F., Marconi A., Cicone C., 2013, *MNRAS*, **433**, 1425
 Bresolin F., 2008, in Israelian G., Meynet G., eds, *The Metal-Rich Universe*. p. 155 ([arXiv:astro-ph/0608410](https://arxiv.org/abs/astro-ph/0608410))
 Curti M., Cresci G., Mannucci F., Marconi A., Maiolino R., Esposito S., 2017, *MNRAS*, **465**, 1384
 Curti M., Mannucci F., Cresci G., Maiolino R., 2020, *MNRAS*, **491**, 944
 Curti M., et al., 2022, *MNRAS*,
 Dere K. P., Del Zanna G., Young P. R., Landi E., Sutherland R. S., 2019, *ApJS*, **241**, 22
 Ellison S. L., Patton D. R., Simard L., McConnell A. W., 2008, *ApJ*, **672**, L107
 Esteban C., Peimbert M., Torres-Peimbert S., Rodríguez M., 2002, *ApJ*, **581**, 241
 García-Rojas J., Esteban C., 2007, *ApJ*, **670**, 457
 Garnett D. R., 1992, *AJ*, **103**, 1330
 Haardt F., Madau P., 2012, *ApJ*, **746**, 125
 Izotov Y. I., Guseva N. G., Fricke K. J., Henkel C., 2019, *A&A*, **623**, A40
 Katz H., 2022, *MNRAS*, **512**, 348
 Katz H., et al., 2022a, *MNRAS*,
 Katz H., et al., 2022b, *MNRAS*, **515**, 4265
 Kewley L. J., Ellison S. L., 2008, *ApJ*, **681**, 1183
 Kewley L. J., Nicholls D. C., Sutherland R. S., 2019, *ARA&A*, **57**, 511
 Kimm T., Katz H., Haehnelt M., Rosdahl J., Devriendt J., Slyz A., 2017, *MNRAS*, **466**, 4826
 Kobulnicky H. A., Kennicutt Robert C. J., Pizagno J. L., 1999, *ApJ*, **514**, 544
 Lequeux J., Peimbert M., Rayo J. F., Serrano A., Torres-Peimbert S., 1979, *A&A*, **80**, 155
 Liu X. W., Luo S. G., Barlow M. J., Danziger I. J., Storey P. J., 2001, *MNRAS*, **327**, 141
 Luridiana V., Morisset C., Shaw R. A., 2015, *A&A*, **573**, A42
 Ma X., Hopkins P. F., Faucher-Giguère C.-A., Zolman N., Muratov A. L., Kereš D., Quataert E., 2016, *MNRAS*, **456**, 2140
 McGaugh S. S., 1991, *ApJ*, **380**, 140

- Palay E., Nahar S. N., Pradhan A. K., Eissner W., 2012, [MNRAS](#), **423**, L35
- Peimbert M., 1967, [ApJ](#), **150**, 825
- Peimbert M., Costero R., 1969, [BOTT](#), **5**, 3
- Peimbert M., Storey P. J., Torres-Peimbert S., 1993, [ApJ](#), **414**, 626
- Pérez-Montero E., 2017, [PASP](#), **129**, 043001
- Sanders R. L., et al., 2022, arXiv e-prints, p. [arXiv:2207.12430](#)
- Stasińska G., 1978, [A&A](#), **66**, 257
- Stasińska G., 1990, [A&AS](#), **83**, 501
- Stasińska G., 2005, [A&A](#), **434**, 507
- Tremonti C. A., et al., 2004, [ApJ](#), **613**, 898
- Yates R. M., Schady P., Chen T. W., Schweyer T., Wiseman P., 2020, [A&A](#), **634**, A107

This paper has been typeset from a \LaTeX file prepared by the author.